MAGNETIC FIELD DEPENDENT VISCOUS FLUID-FLOW BETWEEN SQUEEZING PLATES WITH HOMOGENEOUS AND HETEROGENEOUS REACTIONS

by

Wajid Ullah JAN[a], Muhammad FAROOQ[a*], Jamel BAILI[b,c], Rehan Ali SHAH[d], Aamir KHAN[e], and Hijaz AHMAD[f*]

[a] Department of Mathematics, Abdul Wali Khan University Mardan, Mardan, Pakistan
[b] Department of Computer Engineering, College of Computer Science, King Khalid University, Abha, Saudi Arabia
[c] Higher Institute of Applied Science and Technology of Sousse (ISSATS), Cite Taffala (Ibn Khaldoun) Sousse, University of Souse, Souse, Tunisia
[d] Department of Basic Sciences and Islamiat, University of Engineering and Technology, Peshawar, Pakistan
[e] Department of Pure and Applied Mathematics, The University of Haripur, Haripur, Pakistan
[f] Section of Mathematics, International Telematic University Uninettuno, Roma, Italy

Original scientific paper
https://doi.org/10.2298/TSCI21S2423J

The impacts of magnetic field dependent viscous fluid is explored between squeezing plates in the presence of homogeneous and heterogeneous reactions. The unsteady constitutive equations of heat and mass transfers, modified Navier-Stokes, magnetic field and homogeneous and heterogeneous reactions are coupled as an system of ODE. The appropriate solutions are established for the vertical and axial induced magnetic field equations for the transformed and momentum as well as for the MHD pressure and torque exerted on the upper plate, and are in details. In the case of a smooth plate, the self-similar equation with acceptable starting assumptions and auxiliary parameters is solved by utilising a homotopy analytics method, to generate an algorithm with fast and guaranteed convergence. By comparing homotopy analytics method solutions with BVP4c numerical solver packaging, the validity and correctness of the homotopy analytics method findings are demonstrated. Magnetic Reynolds number have been shown to cause to decrease the distribution of magnetic field, fluid temperature, axial and tangential velocity. The magnetic field also has vertical and axial components with increasing viscosity. The applications of the investigation include car magneto-rheological shock absorbers, modern aircraft landing gear systems, procedures for heating or cooling, biological sensor systems, and bio-prothesis, etc.

Key words: *squeezing plates, magnetic field, Reynolds numbers, BVP4c, homotopy analytics method*

Introduction

The mechanics of fluid movements influenced by the strengths of magnetic polarisation are dealt with by ferrohydrodynamics (FHD). Magnetic fluids have several heat transfer applications using ferrofluids. The liquid cooled speakers that include the tiny volume

* Corresponding authors, e-mail: hijaz555@gmail.com, muhammadfarooq@awkum.edu.pk

of ferrofluid in order to remove heat from the speaker bowls are one of these phanomens Krishnaa *et al.* [1]. This invention improves the spindle's amplifying power, which results in a high-fidelity sound. Magnetic fluids are also used to transport medicines to a specific location in the human body, a magnet field may pilot a drop of ferrofluid in the human body Hooman *et al.* [2]. Under Lenz's law, a driver's movement into a magnetic field induces electric current in the conductor which produces its own magnet field. When a leading fluid moves currents through a magnetic field, a force of Lorentz operates on the fluid. The motion changes the field and vice versa in MHD. The theory is therefore highly non-linear Choi [3]. Liquids or metallic components that can consist of two or more of the metals or non-metals are called alloys in a homogenous or non-homogeneous mixture. These alloys can be used to transmit heat or to convey the specific characteristics of mixtures. Examples of alloys are steel, brass, phosphorous bronze and solder. Beta alloys are mainly utilised in fabrication processes systems, the manufacture systems for cold rolling sheets Karimipour *et al.* [4] investigated Stoke's convective flow issue through a vertical infinite plate in a rotating system system in presence of variable magnetic field. They found that some or all of the factors impact the velocity and temperature of the fluid. Their action therefore changes the rate of transmission of heat and skin friction along the axis. Increased magnetic, *M*, and Eckert number, parameters lead to an increase in the a velocity profiles for free convection cooling and heating in the plate. Nikkhan *et al.* [5] investigated the flux of MHD and the heat transfer over a porous, mass transferred flat plate and found that the component fluid velocity has risen with a time value and Hall parameters. In the presence of heat radiation using the galerkins finite element method. Sheikholeslami *et al.* [6] explored an unstable MHD free-convective couette flow from two vertically permeable platforms. The radiation parameter and the Prandtl number have a higher temperature influence than the velocity of the fluid. The magnetic parameter and the number of Grashof do not affect fluids, on the other hand. In a tilt magnetic field with heat transfer, Nojoomizade *et al.* [7] researched an instable MHD couette flow between the two endless parallel, porous plates. The bottom plate was deemed immobile and permeable. He observed a magnetic increase which leads to a drop in fluid's velocity. Detailed study is also conducted by Suresh *et al.* [8] on squeezing flow with rotating discs under the influences of the magnetic variable field. Momin [9] uses the combined DTM-Pade technique for the simulation of the magnetic squeeze film issue to exhibit an outstanding convergence, stability and adaptability. In the presence of an exponentially falling heat-generation and transverse magnetic field, the objective of the study is to investigate the effects of different electrical conductivity on free convection flows of an electrically conducting fluid and heat transfer via an isothermal vertical non-leading plate. The aerodynamic forces and heat transmission rates may be conveniently modified by applying an appropriate magnetic field.

Mathematical formulation

We suppose an axisymmetric and incompressible viscous fluid squeezed between two parallel plates separated by a distance of $D(t) = l(1-\beta t)^{1/2}$, where l is illustrative of the separation length of the plates at $t = 0$ as illustrated in fig. 1. The two plates are squeezed for $\beta > 0$, till they reach $t = 1$, then the two plates are separated for $\beta < 0$. The lower plate is fixed and the upper plate moves from or to the lower plate. Meekin and Elco [10] states that both plates are regarded to be excellent conductors. Electric forces are significantly less than the magnetic forces and so the current problem is neglected. The induced magnetic field (B_x, B_z), in the fluid is created by the magnetic field well-defined:

$$H_x = \frac{\beta x M_0}{\mu_1(1-\beta t)}, \quad H_z = \frac{\beta M_0}{\mu_2(1-\beta t)}$$

where the magnetic permeability of the outside and inner media between two plates is H_x, H_z and μ_1, μ_2, respectively, and Mo are used to dimensionless.

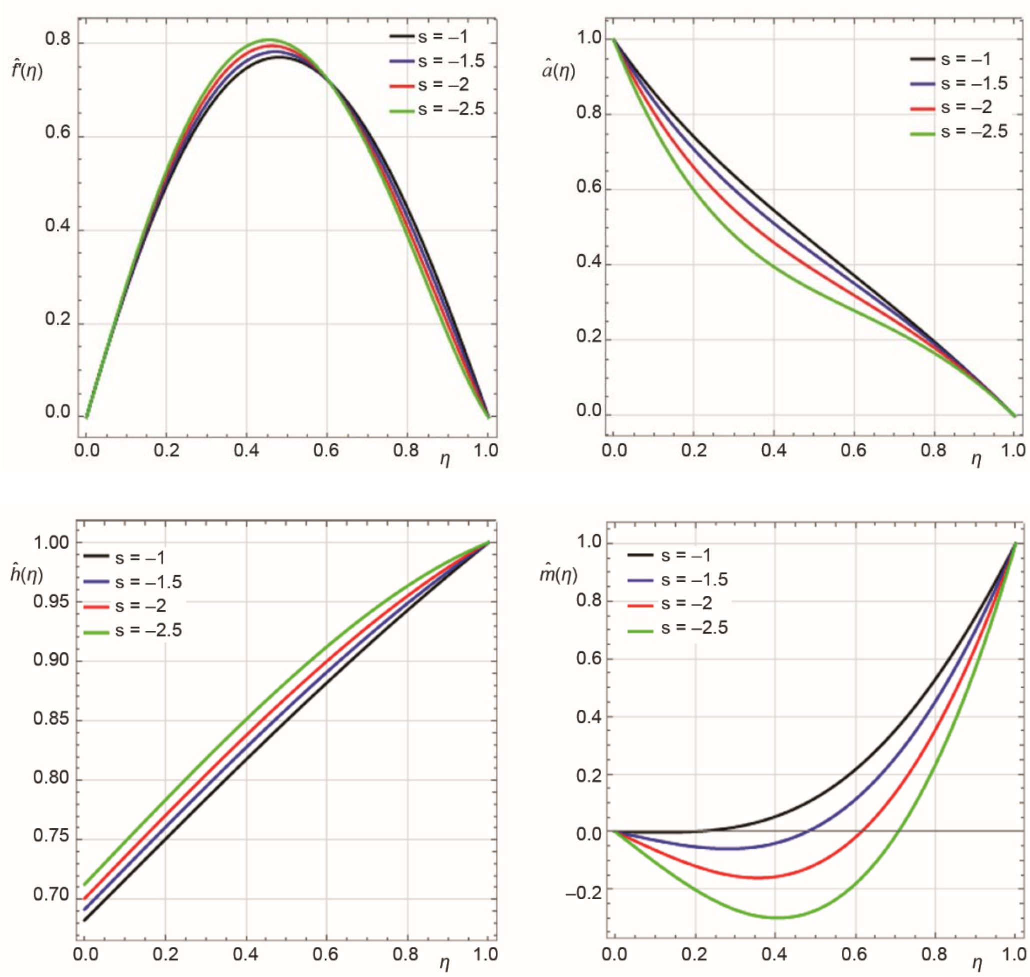

Figure 1. Impact of S for $\hat{f}(\eta)$, $\hat{f}'(\eta)$, $\hat{a}(\eta)$, $\hat{h}(\eta)$, $\hat{g}(\eta)$, and $\hat{m}(\eta)$, with L = 2, δ = 1, Q = 5, K_1 = 2.5, Sc = *Rem* = 2, Pr = 1.8, K_2 = 1.5, *Nc* = 0.2 (*for color image see journal web site*)

The equations which governing the flow and heat/mass transfers in viscous fluid are: Continuity equation is:

$$\nabla \cdot U = 0 \tag{1}$$

Maxwell's equations, simplified for a non-conducting fluid with no displacement currents is:

$$\nabla \cdot B = 0, \quad \nabla \times H = 0 \tag{2}$$

Modified Navier-Stokes equation is:

$$\rho \left[\frac{\partial U}{\partial t} + (\nabla \cdot U)U \right] + \nabla p - \mu \nabla^2 U - \frac{1}{\mu_2}[(\nabla \times B) \times B] = 0 \tag{3}$$

Magnetic field equation is [10-13]:

$$\frac{\partial B}{\partial t} - \nabla \times (V \times B) - \frac{1}{\wp \mu_2} \nabla^2 B = 0 \tag{4}$$

Energy equation:

$$\frac{\partial T}{\partial t} + u\frac{\partial T}{\partial x} + v\frac{\partial T}{\partial y} = \frac{k}{(\rho c_p)}\left(\frac{\partial^2 T}{\partial x^2} + \frac{\partial^2 T}{\partial y^2}\right) + \frac{1}{(\rho c_p)}\frac{16\sigma^* T_0^3}{3\kappa^*}\frac{\partial^2 T}{\partial y^2} + \frac{Q^*}{(\rho c_p)}(T - T_0) \tag{5}$$

Homogeneous/heterogeneous equations:

$$\frac{\partial a}{\partial t} + u\frac{\partial a}{\partial x} + v\frac{\partial a}{\partial y} = D_A \frac{\partial^2 a}{\partial y^2} - K_c a b^2 \tag{6}$$

$$\frac{\partial b}{\partial t} + u\frac{\partial b}{\partial x} + v\frac{\partial b}{\partial y} = D_B \frac{\partial^2 b}{\partial y^2} + K_c a b^2 \tag{7}$$

The squeezing flow under consideration has the following boundary conditions:

$$\begin{gathered} u = 0, \quad w = 0, \quad T = T_l, \quad D_A \frac{\partial a}{\partial y} = k_3 a, \quad D_B \frac{\partial b}{\partial y} = -k_3 a \quad \text{at} \quad y = 0 \\ u = 0, \quad w = \frac{-\alpha D}{2\sqrt{1-\alpha t}}, \quad T = T_u, \quad a = a_0 \quad b = 0 \quad \text{at} \quad y = h(t) \end{gathered} \tag{8}$$

Use the transformations [2]:

$$u = \frac{\beta x \hat{f}'(\eta)}{2(1-\beta t)^2}, \quad w = \frac{-\beta l \hat{f}(\eta)}{(1-\beta t)}, \quad B_x = \frac{\beta x M_0}{2(1-\beta t)}\hat{m}'(\eta)$$

$$B_z = \frac{\beta M_0}{l\sqrt{(1-\beta t)}}\hat{m}(\eta), \quad \eta = \frac{z}{l\sqrt{1-\beta t}}$$

and

$$a = a_0 \hat{h}(\eta), \quad b = a_0 \hat{g}(\eta), \quad T = \hat{a}(\eta) T_{\hat{h}}, \quad \hat{a} = \frac{T - T_u}{T_l - T_u}$$

The continuity equation is satisfied field, heat transfer, homogeneous, and heterogeneous equations takes the following form:

$$\begin{gathered}\hat{f}'''' - 2S_q N_c(\eta \hat{f}''' + 3\hat{f}'' - \hat{f}\hat{f}''' - \hat{f}\hat{f}'') + 6S_q N_c \hat{m}\hat{m}' + \\ +2S_q N_c[2Rem(\eta \hat{m}\hat{m}' + \hat{m}\hat{m}' + \hat{f}\hat{m}\hat{m}' + \hat{f}\hat{m}^2)] = 0\end{gathered} \tag{9}$$

$$\hat{m}'' - Rem(\eta \hat{m}' + \hat{m} - 2\hat{f}\hat{m}' + 2\hat{f}'\hat{m}) = 0 \tag{10}$$

$$\hat{a}''\left(1 + \frac{4}{3}R\right) + \Pr S_q(\hat{f}\hat{a}' - 2\eta \hat{a} + Q\hat{a}) = 0 \tag{11}$$

$$\hat{h}'' - \mathrm{Sc}K_1\hat{h}\hat{g}^2 - \mathrm{Sc}S_q(\eta \hat{h}' - \hat{f}\hat{h}) = 0 \tag{12}$$

$$\hat{g}''\delta - \mathrm{Sc}K_1\hat{h}\hat{g}^2 - \mathrm{Sc}S_q(\eta \hat{g}' - \hat{f}\hat{g}') = 0 \tag{13}$$

The Prandtl number is a dimensionles number which is defined as the ratio of momentum diffusivity (kinematic viscosity) to thermal diffusivity and the boundary conditions are reduced to:

$$\begin{gathered}\hat{f}(0) = 0, \quad \hat{f}'(0) = 0, \quad \hat{m}(0) = 0, \quad \hat{a}(0) = 1, \quad \hat{h}'(0) = K_2\hat{h}(0), \quad \delta\hat{g}'(0) = -K_2\hat{h}(0), \\ \hat{f}(1) = 0.5, \quad \hat{f}'(1) = 0, \quad \hat{m}(1) = 1, \quad \hat{a}(1) = 0, \quad \hat{h}(1) = 1 \quad \hat{g}(1) = 0\end{gathered} \tag{14}$$

Error analysis

The current problem is solved for a specified maximum residual error of 10^{-40}. For an analysis of the error, the HAM is utilised. The analyses are performed using approximations of the 40th order. The authentication of HAM for various physical parameter values is derived from fig. 1 and tabs. 1-3. Figure 1 demonstrates a virtually constant reduction of maximum average residual errors of $\hat{f}(\eta)$, $\hat{m}(\eta)$, $\hat{a}(\eta)$, $\hat{h}(\eta)$, and $\hat{g}(\eta)$ to 17th approximation order. Table 1 presents optimal values of the parameter for the convergence control vs the various approximation orders. At several approximate orders tab. 2 illustrates the individual average squared residual error. Table 3 shows that the numerical values of $\hat{f}''(0)$, $-\hat{m}'(0)$, $-\hat{a}'(0)$, $-\hat{h}'(0)$, and $-\hat{g}'(0)$ almost converge at the 5th order of approximation.

Table 1. Total residual error of $\hat{f}(\eta), \hat{m}(\eta), \hat{a}(\eta), \hat{h}(\eta)$, and $\hat{g}(\eta)$ with Pr = 0.5, S = –0.5, L = 0.01, Q = 5, R = 0.7, δ = 1, Sc = 2.5, K_1 = 0.1, K_2 = 1, Ha = 0.1, and M = 0.3

n	$\epsilon^{\hat{f}}n$	$\epsilon^{\hat{m}}n$	$\epsilon^{\hat{a}}n$	$\epsilon^{\hat{h}}n$	$\epsilon^{\hat{g}}n$
2	8.44617×10^{-7}	1.24624×10^{-7}	8.47003×10^{-12}	5.6788×10^{-9}	3.90679×10^{-12}
10	2.2244×10^{-25}	1.6628×10^{-25}	2.21163×10^{-32}	1.81546×10^{-31}	2.06285×10^{-34}
20	5.63643×10^{-32}	1.41176×10^{-33}	1.19048×10^{-33}	2.31112×10^{-34}	3.64121×10^{-36}
30	5.63643×10^{-32}	1.41176×10^{-33}	1.19048×10^{-33}	2.31112×10^{-34}	3.64121×10^{-36}
40	5.63643×10^{-32}	1.41176×10^{-33}	1.19048×10^{-33}	2.31112×10^{-34}	3.64121×10^{-36}

Table 2. Computational of $\hat{f}(\eta), \hat{m}(\eta), \hat{a}(\eta), \hat{h}(\eta)$, *and* $\hat{g}(\eta)$, when *Sq* = –0.5, Pr = 2, *Rem* = 0.1, δ = 1, *Q* = 3.5, *R* = 5, Sc = 7, K_1 = 5, K_2 = 0.1, *Nc* = 2

HAM result						Numerical result				
η	$\hat{f}(\eta)$	$\hat{m}(\eta)$	$\hat{a}(\eta)$	$\hat{h}(\eta)$	$\hat{g}(\eta)$	$\hat{f}(\eta)$	$\hat{m}(\eta)$	$\hat{a}(\eta)$	$\hat{h}(\eta)$	$\hat{g}(\eta)$
0	0	0	1.0000	0.4756	0.2481	0	0	1.0000	0.4756	0.2481
0.2002	0.0538	0.1931	0.7843	0.5839	0.1698	0.0538	0.1931	0.7843	0.5839	0.1698
0.4004	0.1817	0.3881	0.5810	0.6999	0.1162	0.1817	0.3881	0.5810	0.6999	0.1162
0.6006	0.3312	0.5870	0.3851	0.8068	0.0734	0.3312	0.5870	0.3851	0.8068	0.0734
1.0000	0.5000	1.0000	0.0000	1.0000	–0.0000	0.5000	1.0000	0.0000	1.0000	–0.0000

Table 3. Convergence of the homotopy solution for different orders of approximation for $\hat{f}''(\eta), -\hat{m}'(\eta), -\hat{a}'(\eta), -\hat{h}'(\eta)$, and $-\hat{g}'(\eta)$ when *Sq* = –0.5, Pr = 2, *Rem* = 0.1, δ = 1, *Q* = 3.5, *R* = 5, Sc = 7, K_1 = 5, K_2 = 0.1, *Nc* = 2 and different values of η

η	$\hat{f}(\eta)$	$-\hat{m}(\eta)$	$-\hat{a}(\eta)$	$-\hat{h}(\eta)$	$-\hat{g}(\eta)$
0	3.0638	–0.9630	1.1182	–0.4756	0.4756
0.2002	1.8605	–0.9675	1.0418	–0.5807	0.3175
0.4004	0.5335	–0.9823	0.9930	–0.5636	0.2303
0.6006	–0.7347	–1.0063	0.9679	–0.5039	0.2038
0.8008	–1.8304	–1.0347	0.9619	–0.4766	0.1890
1.0000	–2.6899	–1.0594	0.9696	–0.4888	0.1462

Results and discussions

The influence of the involved physical parameters is shown both graphically and numerically through tables for the velocity components $\hat{f}(\eta)$ magnetic field components $\hat{m}(\eta)$, temperature variation $\hat{a}(\eta)$, and homogeneous-heterogeneous variation $\hat{h}(\eta)$, and $\hat{g}(\eta)$. Figure 1 show the influence of *Sq* on $\hat{f}'(\eta)$, $\hat{a}(\eta)$, $\hat{h}(\eta)$, and $\hat{m}(\eta)$. The distance between the plates is increasing, that is $Sq = -1, -1.5, -2, -2.5$, the fluid will flow into the *X*-axis direction with fixed values of other parameters which is set to reduce the velocity $\hat{f}'(\eta)$, however when the fluid goes through the central area, it start increasing, Furthermore, this phenomenon reduces velocity as the squeezing impact is dominated by velocity. Figures shows that fluid friction is caused by the squeezing of plates, which generates heat and increases the temperature of the fluid.

The concentration profiles $\hat{f}(\eta)$, $\hat{m}(\eta)$, $\hat{a}(\eta)$, and $\hat{g}(\eta)$ decrease and $\hat{f}'(\eta)$ and $\hat{h}(\eta)$ increases, it is observed that due to increase in *Sq*. According to this an increase in the homogeneous chemical reaction, which decreases viscosity. However, the $\hat{h}(\eta)$ indicates the reverse of the $\hat{g}(\eta)$ above can be seen in fig. 1.

Figure 2 is drawn to show the effect of the magnetic Reynolds number, *Rem*, and *Nc* on $\hat{f}(\eta)$ and $\hat{m}(\eta)$. The magnetic Reynolds number characterizes the proportion of the liquid transition to the magnetic diffusivity. The boundary, therefore, is instrumental in deciding the dissemination of the e magnetic field along the streamlines. Expanding the worth *Rem* = 1.5, 1.6, 1.7, 1.7, for slow vertical velocity of the upper plate, for example *Sq* = –2.5, the axial velocity diminishes while the upward velocity increments after the focal area. The pivotal and vertical initiated magnetic field segments $\hat{m}(\eta)$ decline with the expansion in *Rem*. The maximum value of $\hat{m}(\eta)$ is seen at the upper plate, for example at η = 1.5, which implies that, for higher upsides of *Rem*, the squeeze fluid should have much higher electrical conductivities.

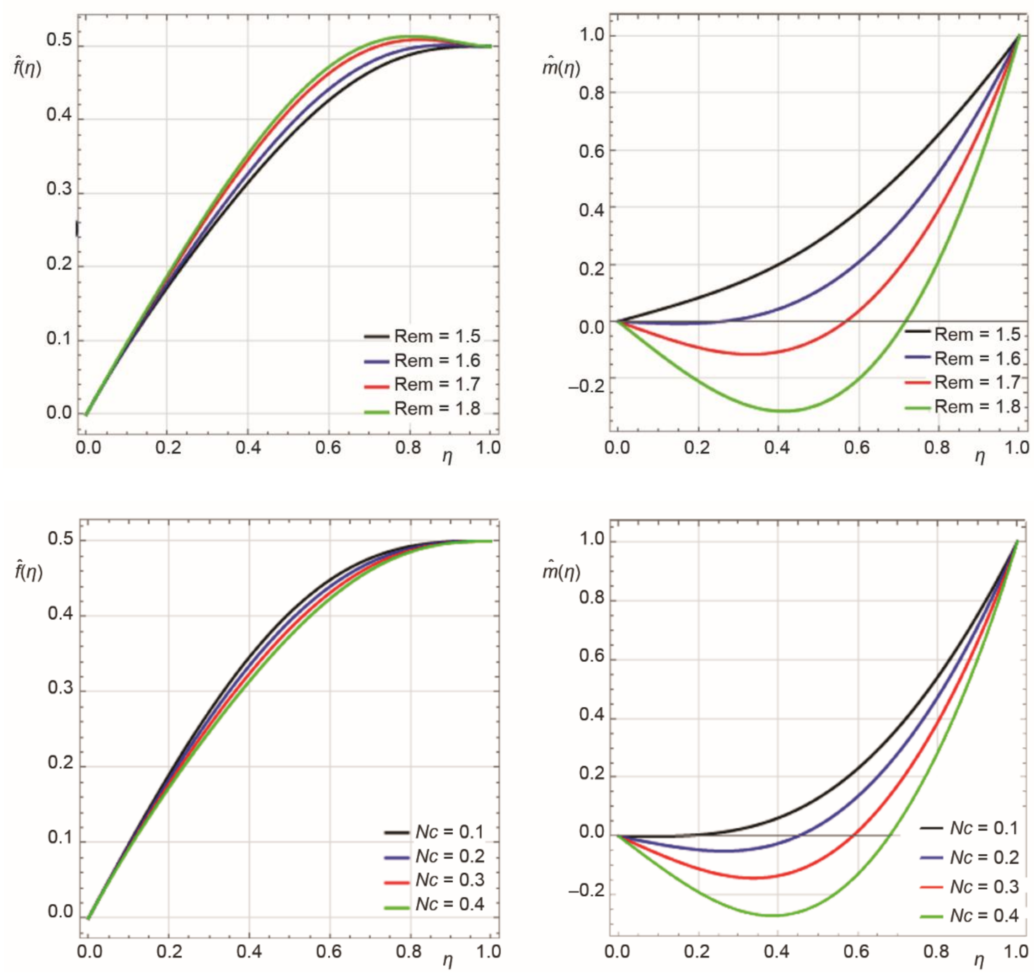

Figure 2. Impact of *Rem* for $\hat{f}(\eta)$ and $\hat{m}(\eta)$ with *L* = 2, δ = 1, *Q* = 5, K_1 = 2.5, *S* = –2.5, Sc = 2, Pr = 1.8, K_2 = 1.5, *Nc* = 0.2

Figures 2(b) and 2(c) depicts effect of *Nc* on $\hat{f}(\eta)$ and $\hat{m}(\eta)$ is the dimensionless strength of axial magnetic field. It is clear from figures, when fluid moves toward upper plate $\hat{f}(\eta)$ start increasing near the mid of fluid domain which again start decreasing as it moves toward upper plate. Similarly $\hat{m}(\eta)$ is decreasing with increase in *Nc*. Maximum decrease is seen at the central region of fluid domain.

The impacts of K_1 and K_2 homogeneous-heterogeneous chemical reaction parameters on concentration profile $\hat{f}(\eta)$, $\hat{h}(\eta)$, $\hat{g}(\eta)$, and $\hat{m}(\eta)$ can be seen in fig. 3.

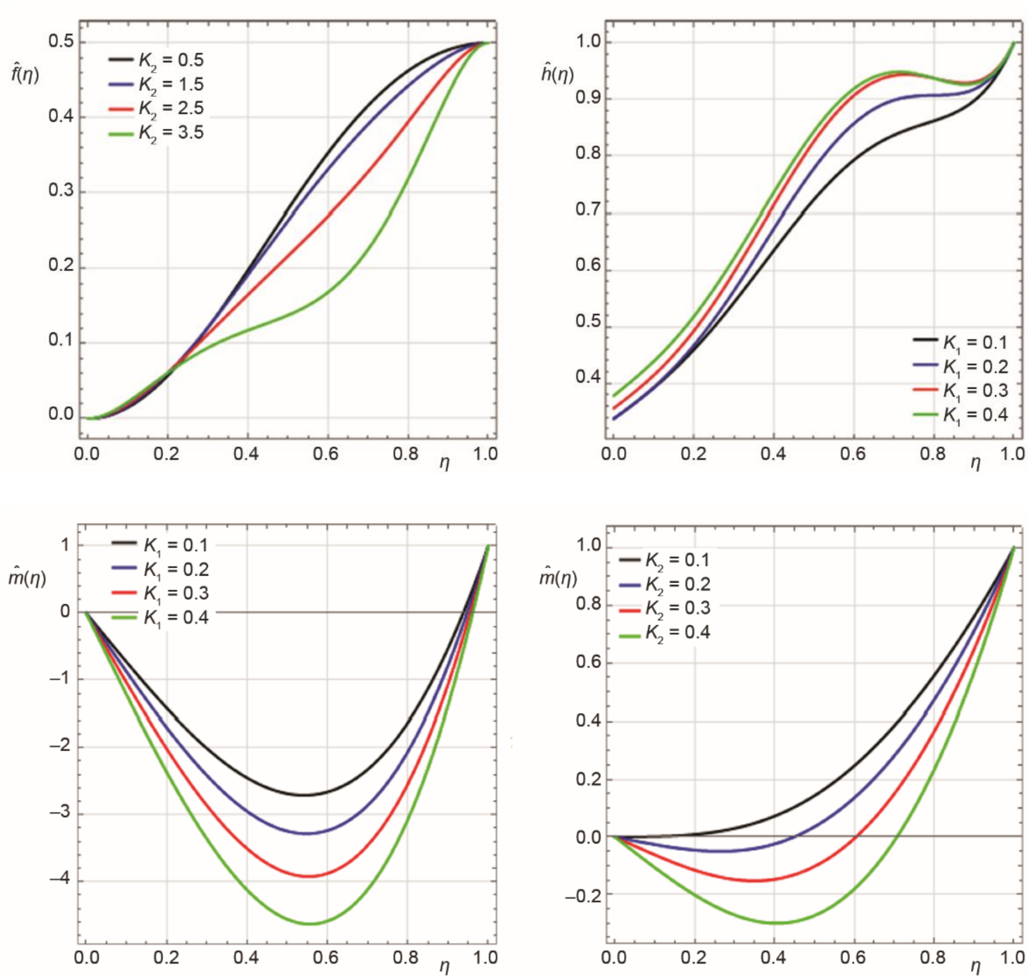

Figure 3. Impact of K_1 and K_2 for $\hat{f}(\eta)\hat{h}(\eta)$ with L = 2, δ = 1, Q = 5, R = 2.5, S = –2.5, Rem = 2, Nc = 0.2, Pr = 1.8, Sc = 2

It is seen that an increment in K_1 show to an increment in $\hat{f}(\eta)$ and $\hat{h}(\eta)$. This is because of the way that the consistency decreases with an increment in the homogeneous chemical reaction parameter. However, the heterogeneous boundary K_2 shows inverse outcome to above, which is displayed in figure. This is a direct result of the diffusion reduces with a decline in K_2 and less diffused particles will ascend in the concentration.

The impacts of the strength of homogeneous response K_1 on concentration field $\hat{m}(\eta)$ is depicted. As the reactants are down in a chemical reaction. In view of this reality concentration feld shows inclination the propensity for further developing values of K_1. It is seen that concentration dissemination is the diminishing capacity of the strength of heterogeneous reaction K_2. Higher values of K_2 enervate the diffusion coefficient and thus, less diffused particles subside the concentration feld.

Conclusion

The main upshots of this study are given as follows.

- Table 1 shows total residual error of $\hat{f}'(\eta)$, $\hat{m}(\eta)$, $\hat{a}(\eta)$, $\hat{h}(\eta)$, and $\hat{g}(\eta)$.
- Table 2 shows that HAM and BVP4c match efectively with the values of $\hat{f}(\eta)$, $\hat{m}(\eta)$, $\hat{a}(\eta)$, $\hat{h}(\eta)$, and $\hat{g}(\eta)$.
- Table 3 shows the convergence of the homotopy solution for diferent orders of approximation.
- The homogeneous and heterogeneous reaction strength parameters assist to control the concentration profiles of the flow.

Acknowledgment

The Authors extend their thanks to the Deanship of Scientific Research at King Khalid University for funding this work through the big research groups under grant number RGP. 1/155/42.

Reference

[1] Krishnaa, M. V., *et al.*, Hall and Ion Slip Effects on Unsteady MHD Free Convective Rotating Flow Through a saturated Porous Medium over an Exponential Accelerated Plate, *Alex. Eng. J., 59* (2020), 2, pp. 565-577
[2] Hooman, K., *et al.*, A Theoretical Model to Predict Gas Permeability for Slip Flow Through a Porous Medium, *Appl. Therm. Eng., 70* (2014), 1, pp. 71-76
[3] Choi, S. U. S., Enhancing Thermal Conductivity of Fluids with Nanoparticles, *ASME FED., 66* (1995), Nov., pp. 99-105
[4] Karimipour, A., *et al.*, Simulation of Copper-Water Nanofluid in a Microchannel in Slip Flow Regime Using the Lattice Boltzmann Method, *Eur. J. Mech. B. Fluids, 49 (2015)*, Jan.-Feb., pp. 89-99
[5] Nikkhah, Z., *et al.*, Forced Convective Heat Transfer of Water/Functionalized Multi-Walled Carbon Nanotube 2 Nanofluids in a Microchannel with Oscillating Heat Flux and Slip Boundary Condition, *Int. Commun. Heat Mass., 68* (2015), Nov., pp. 69-77
[6] Sheikholeslami, M., *et al.*, Heat Transfer Simulation of Heat Storage Unit with Nanoparticles and Fins Through a Heat Exchanger, *Int. J. Heat Mass. Transf., 135* (2019), June, pp. 470-478
[7] Nojoomizade, M., *et al.*, Investigation of Permeability Effect on Slip Velocity and Temperature Jump Boundary Conditions for FMWNT/Water Nanofluid Flow and Heat Transfer Inside a Microchannel Filled by a Porous Media., *Physica E, 97* (2018), Mar., pp. 226-238
[8] Suresh, S., *et al.*, Synthesis of AL_2O_3-Cu/Water Hybrid Nanofluids Using Two Step Method and Its Thermophysical Properties, *Colloid Surface A, 388* (2011), 1, pp. 41-48
[9] Momin, G. G., A Experimental Investigation of Mixed Convection with Water-AL_2O_3 Hybrid Nanofluid in Inclined Tube for Laminar Flow, Int. J. Sci. Technol. Res., 2 (2013), 12, pp. 195-202
[10] Merkin, J. H., A Model for Isothermal Homogeneous-Heterogeneous Reactions in Boundary-Layer Flow, *Math. Comput. Modelling., 24* (1996), 8, pp. 125-136
[11] Ramana Reddy, J. V., *et al*., Effect of Frictional Heating on Radiative Ferro Fluid Flow Over a Slendering Stretching Sheet with Aligned Magnetic Field, *The Eur. Phys. J. Plus., 132* (2017), 7, pp. 1-13
[12] Ramana Reddy, J. V., *et al*., Effect of Non-Linear Thermal Radiation on MHD Flow between Rotating Plates with Homogeneous-Heterogeneous Reactions, *Int. J. Engin. Res. in Africa., 20* (2015), Oct., pp. 130-143
[13] Jawad, R., *et al*., Numerical Investigation of Copper-Water (Cu-Water) Nanofluid with Different Shapes of Nanoparticles in a Channel with Stretching Wall Slip Effects, *Math. Comput. Appl., 21* (2016), 4, pp. 43-58

Paper submitted: July 10, 2021
Paper revised: July 28, 2021
Paper accepted: August 8, 2021